Pressure-induced rotation of spontaneous polarization in monoclinic and triclinic $PbZr_{0.52}Ti_{0.48}O_3$

J. Rouquette, J. Haines,* V. Bornand, M. Pintard, and Ph. Papet
Laboratoire de Physico-Chimie de la Matière Condensée, UMR CNRS 5617, Université Montpellier II, Place Eugène Bataillon, cc003, 34095 Montpellier cedex 5, France

W. G. Marshall and S. Hull
ISIS Facility, Rutherford Appleton Laboratory, Chilton, Didcot, Oxfordshire, OX11 0QX, United Kingdom
(Received 25 June 2004; revised manuscript received 15 September 2004; published 21 January 2005)

The morphotropic composition of lead zirconate titanate (PZT), $PbZr_{0.52}Ti_{0.48}O_3$, was studied as a function of temperature (47–310 K) and hydrostatic pressure (from 0.1 MPa to 7.6 GPa) by neutron powder diffraction. Series of monoclinic (space groups *Cm* and *Cc*) and triclinic phases (space groups *F*1 and $F\bar{1}$) were observed at various points in the *P*-*T* phase diagram of $PbZr_{0.52}Ti_{0.48}O_3$. The high-pressure behavior is characterized by two mechanisms, a rotation and reduction of the spontaneous polarization and the onset of octahedral tilting leading to unit cell doubling. The results show that pressure, as in the case of temperature and external electric fields, can induce polarization rotation.

DOI: 10.1103/PhysRevB.71.024112 PACS number(s): 77.84.Dy, 61.50.Ks, 62.50.+p, 61.12.Ld

I. INTRODUCTION

Lead-based ferroelectric perovskites represent an important class of piezoelectric materials. Due to their high piezoelectric performances, lead-zirconate–lead-titanate solid solutions $PbZr_{1-x}Ti_xO_3$ (PZT) with x values close to 0.48 are of particular interest. This composition lies on what is termed the morphotropic phase boundary (MPB) between the ferroelectric trigonal (space group *R*3*m*) and tetragonal phases (space group *P*4*mm*). The high piezoelectric coupling constants in these materials have long been attributed to the simultaneous presence of trigonal and tetragonal domains near the MPB.[1] Recently, it has been shown that there is in fact a monoclinic phase [space group *Cm* (Refs. 2–4)] in this region of the phase diagram. The polar axis of this phase can lie anywhere between the pseudocubic [001] and [111] directions, thus providing a polarization rotation mechanism[5,6] as a possible origin for the high piezoelectric response. A second monoclinic phase [space group *Cc* (Refs. 7–9)] with a doubled unit cell due to antiferrodistortive tilting of the $(Zr,Ti)O_6$ octahedra has been observed below 210 K at ambient pressure in $PbZr_{0.52}Ti_{0.48}O_3$ based on the appearance of superlattice reflections in electron and neutron diffraction data.

The origin of the stability of the monoclinic phase is still a subject of discussion. From a theoretical point of view, Devonshire theory has to be expanded to eighth order in order for the monoclinic phase to be allowed.[10] Recent Raman scattering[11] and electron diffraction studies[12] indicate that on a local level the structure of PZT is monoclinic over a very wide compositional range due to off-center lead displacements. Condensation of these displacements leads to the formation of the observed, long-range monoclinic structure. Neutron diffraction results[13,14] show that the monoclinic phase exhibits *hkl*-dependent broadening of the diffraction lines, which has been related to spatial variation of the Zr/Ti ratio. In the same study,[13] it was predicted that in the absence of spatial inhomogeneity the monoclinic phase would disappear; however, spatial inhomogeneity is probably unavoidable in the PZT solid solution. It can also be noted[4,13,15,16] that very often a second phase (*R*3*m* or *P*4*mm*) coexists with the monoclinic form. The phases observed for a given sample will be highly dependent on the exact chemical composition, spatial inhomogeneity, and method of synthesis.

In addition to the ongoing investigation of the relatively well-studied, highly complex, composition-temperature phase diagram of PZT, it is also very important to understand the effect of hydrostatic pressure on the phase diagram of this material. This is of particular interest as the dielectric and piezoelectric properties of PZT ceramics, which depend on the nature of the phases present and on domain wall motion, are known to be sensitive to stress induced by external elastic or electric fields. Previous studies[17–23] on $PbZr_{0.52}Ti_{0.48}O_3$ by x-ray diffraction, Raman spectroscopy, and dielectric measurements indicate that the stable forms at high pressure are the monoclinic *Cc* form and a pseudocubic form. The latter is characterized by cubic unit-cell parameters and a strong Raman spectrum, which is not consistent with the cubic paraelectric form found at high temperature and ambient pressure. A different high-pressure phase transition sequence involving rhombohedral forms (*Cm*-*R*3*m*-*R*3*c*) was proposed, based on a subsequent investigation[24] using x-ray diffraction, Raman spectroscopy, and theoretical methods. The monoclinic *Cm* and *Cc* forms have also been observed at high pressure by neutron diffraction in Ti-rich PZT compositions, which are tetragonal under ambient conditions.[25] Up to now, the structures of the high-pressure forms of $PbZr_{0.52}Ti_{0.48}O_3$ have not been determined. The high-pressure behavior and crystal structures of $PbZr_{0.52}Ti_{0.48}O_3$ may be expected to be particularly complex due to the possible coexistence of rotational and ferroelectric lattice distortions for compositions close to the MPB (Ref. 26) linked respectively to R_4^+- and Γ_4^--type phonons.[27] In the present study, the structure of $PbZr_{0.52}Ti_{0.48}O_3$ is refined at several (P,T) points in the pressure-temperature phase diagram of PZT in order to determine the phase transition se-

TABLE I. Cell parameters for monoclinic and triclinic $PbZr_{0.52}Ti_{0.48}O_3$ as a function of P and T.

P(GPa)	T(K)	a(Å)	b(Å)	c(Å)	α(deg)	β(deg)	γ(deg)	V(Å^3)
0.0001	47	10.0067(2)	5.7033(1)	5.7149 (1)	90	124.335(1)	90	269.321(8)
0.0001	150	10.0138(2)	5.7057(1)	5.7167 (1)	90	124.367(1)	90	269.611(8)
0.0001	230	5.7160(1)	5.7094(1)	4.1342 (1)	90	90.387(2)	90	134.915(3)
0.0001	280	5.7166(1)	5.7106(1)	4.1342 (1)	90	90.347(2)	90	134.958(3)
0.7	150	9.9784(7)	5.7007(3)	5.7200 (4)	90	124.59(3)	90	267.86(3)
1.1	280	5.7113(3)	5.7089(3)	4.0944 (3)	90	90.356(7)	90	133.50(1)
2.4	281	9.8953(6)	5.6973(3)	5.7067 (3)	90	124.995(3)	90	263.56(3)
3.8	288	8.0597(4)	8.0291(3)	8.0546(4)	90.141(13)	90.186(9)	90.051(11)	521.23(4)
4.9	295	8.0400(4)	8.0072(3)	8.0298(4)	90.224(7)	90.122(11)	90.067(10)	516.94(4)
7.2	128	7.9894 (3)	7.9544 (4)	7.9821(4)	90.265 (8)	90.114(10)	90.139(14)	507.27(4)
7.1	306	7.9895(4)	7.9637(4)	7.9850 (4)	90.208(10)	90.105(12)	90.110(16)	508.05 (5)
7.6	310	7.9779(4)	7.9518(4)	7.9787(4)	90.267(10)	90.093(11)	90.198(12)	506.16(5)

quence of this material and to investigate the relative roles of rotation and reduction of the spontaneous polarization and octahedral tilting at high pressure.

II. EXPERIMENT

$PbZr_{0.52}Ti_{0.48}O_3$ was prepared by the conventional solid-state reaction from high-purity (>99.9%) oxides via a two-stage calcination process.[17,18] The resulting powder samples were analyzed by inductively coupled plasma and electron microprobe analysis. The following Pb:Zr:Ti compositional ranges were found: respectively, 1.00(1):0.52(1):0.48(1) and 1.00(1):0.53(1):0.47(1). Ambient-pressure, time-of-flight neutron diffraction data at room temperature and at low temperature were first obtained using an orange cryostat on the Polaris medium resolution diffractometer at the ISIS spallation source of the Rutherford Appleton Laboratory. The 21.8-g sample was placed in a 10-mm-diam standard vanadium sample can in the cryostat. Data were collected using detector banks centered at $2\theta=90°$ (ZnS scintillators) and $2\theta=145°$ (^{3}He ionization counters). The acquisition time was of the order of 4 h. The data were corrected for absorption.

$PbZr_{0.52}Ti_{0.48}O_3$ was then studied as a function of temperature (128–310 K) and pressure (0.7–7.6 GPa) in a Paris-Edinburgh pressure cell, which was placed in a liquid nitrogen cryostat, on the high-pressure facility (HiPr) of the PEARL beamline at ISIS. The sample was loaded into an encapsulated null-scattering TiZr gasket with deuterated 4:1 methanol:ethanol as a pressure-transmitting medium. The pressure was estimated based on the thermoelastic equation of state (EOS) of lead,[28] which had also been introduced into the sample volume. The pressure variation was obtained based on a third-order Birch-Murnaghan EOS (Ref. 29) with an ambient temperature bulk modulus $B_0=41.84$ GPa and first pressure derivative $B_0'=5.72$. The temperature variation was introduced by modifying the value of V_0 due to thermal expansion. $B_0(T)$ is modeled by a quadratic in T and $B_0'(T)$ by a simple linear expression. The temperature was measured with a type-K thermocouple attached to the rear anvil of the cell. The temperature stability was better than ±2 K. Pressure was always increased at close to ambient temperature, at which the deuterated 4:1 methanol:ethanol remains liquid in the pressure range studied in order to limit reflection-broadening problems due to vitrification of the pressure transmitting fluid, which occurs at low temperature. Low-temperature points (128 K, 150 K) were thus always obtained along isobars. Data were collected at a diffraction angle $2\theta=90°$ using a bank of ZnS scintillator detectors. Data acquisition times were of the order of 10 h. The data were normalized with respect to those of a standard vanadium sample and corrected for incident beam attenuation due to the tungsten carbide anvils of the pressure cell.

Structure refinements were performed with the Rietveld refinement program GSAS (Ref. 30). Four phases were included in the refinements of the high-pressure data: PZT, tungsten carbide and nickel (from the anvils of the pressure cell), and lead. In the refinements, the cell parameters, atomic positions, atomic displacement parameters, scale factor, and line shape parameters were varied along with up to 15 background parameters. The data were first refined using isotropic atomic displacement parameters. Anisotropic atomic displacement parameters were also refined for the lead and oxygen atoms of PZT. Symmetry- and *hkl*-dependent anisotropic microstrain parameters as implemented in GSAS line shape 4 were also included.[30,31] In recent studies,[13,14] this line shape function was found to be particularly well suited to model the microstrain present in PZT ceramics. All figures in parentheses refer to estimated standard deviations.

III. RESULTS AND DISCUSSION

A. Variable-temperature study of $PbZr_{0.52}Ti_{0.48}O_3$

The diffraction data obtained as a function of temperature at ambient pressure confirmed the presence of the ambient-temperature (Cm) and low-temperature (Cc) monoclinic forms in $PbZr_{0.52}Ti_{0.48}O_3$, Tables I and II. The structural data are similar to those reported in previous studies.[9,15] As is

TABLE II. Fractional atomic coordinates, isotropic (iso), or equivalent (eq) atomic displacement parameters (Å^2) and agreement factors (%) for monoclinic $PbZr_{0.52}Ti_{0.48}O_3$ as a function of *T*. *Cm*: site occupancies Pb, Zr/Ti, O(1) $2a(x,0,z)$, O(2) $4b(x,y,z)$. Origin at Pb position. *Cc*: site occupancies $4a(x,y,z)$. Origin based on Pb *x* and *z* coordinates $(0,y,0)$.

	Cc	*Cc*	*Cm*	*Cm*
T(K)	47	150	230	280
y-Pb	0.7420(2)	0.7428(3)	0	0
U_{eq}-Pb	0.012(1)	0.0148(2)	0.0178(2)	0.0195(2)
x-Zr, Ti	0.2192(2)	0.2193(2)	0.4783(5)	0.4815(6)
y-Zr,Ti	0.2596(7)	0.2598(7)	0	0
z-Zr,Ti	0.1921(4)	0.1951(4)	0.5623(3)	0.5619(4)
U_{iso}-Zr	0.0050(1)	0.0052(1)	0.0047(1)	0.0043(1)
U_{iso}-Ti	0.0196(5)	0.0170(5)	0.0084(3)	0.0076(3)
x-O(1)	−0.0433(1)	−0.0431(1)	0.4675(3)	0.4698(3)
y-O(1)	0.2439(6)	0.2455(8)	0	0
z-O(1)	−0.0840(2)	−0.0806(2)	0.0871(2)	0.0861(3)
U_{eq}-O(1)	0.0089(4)	0.0104(7)	0.0107(3)	0.0115(3)
x-O(2)	0.1955(3)	0.1954(1)	0.2209(2)	0.2231(3)
y-O(2)	0.4861(1)	0.4888(3)	0.2450(2)	0.2451(3)
z-O(2)	−0.1016(3)	−0.0959(3)	0.6102(2)	0.6089(2)
U_{eq}-O(2)	0.0066(3)	0.0075(3)	0.0105(3)	0.0110(2)
x-O(3)	0.1921(1)	0.1944(1)		
y-O(3)	0.0033(3)	0.0013(4)		
z-O(3)	0.4170(3)	0.4205(3)		
U_{eq}-O(3)	0.0094(2)	0.0113(3)		
R_{wp}	3.8	4.2	4.0	4.0
R_p	4.2	4.0	4.0	4.2

commonly encountered for samples which lie on the morphotropic phase boundary, the line shape of many reflections is complex. The reflections are broader than those of nonmorphotropic samples. If one takes the pseudocubic 200 and 002 reflections, for example, even though these reflections are well separated for $PbZr_{0.52}Ti_{0.48}O_3$, the intensity does not descend to the background level over the interval between them as has been observed in previous studies. This behavior has in the past been attributed to either the presence of a second phase (most commonly the rhombohedral form) or to the presence of diffuse scattering due to disorder. In the present study, the scattering between the 200 and 002 reflections had no well-defined structure that could be associated with a reflection arising from a second phase. Two-phase refinements ($Cm+R3m$) thus did not improve the fit to the data. The best fits were obtained using single-phase *Cm* or *Cc* with microstrain broadening to account for the distorted line shapes due to true microstrain and also to different relative contributions under the peaks corresponding to different classes of reflections due to diffuse scattering. Typical values of the S_{HKL} parameters used to model the microstrain are given in Table III.

The presence of a single phase is in contrast with previous neutron powder diffraction results on $PbZr_{0.52}Ti_{0.48}O_3$ (Ref. 15) and $PbZr_{0.53}Ti_{0.47}O_3$ (Ref. 16), for which the tetragonal and rhombohedral forms were found to be present, respectively. This distinct behavior in the present study would appear to be due to slight differences in composition. It has been shown that the c/a ratio for the elementary perovskite unit cell depends closely on the composition in the $PbZr_{1-x}Ti_xO_3$ solid solution.[4,16] The value obtained for the present sample (1.023) is intermediate with respect to those studied in Ref. 15 (1.026) and Ref. 16 (1.019), indicating that the composition of the present sample is also intermediate. This would be in agreement with the chemical analysis results (see Experiment section). In the present circumstances, it appears that the composition studied lies intermediate between those, which were found to exhibit tetragonal and rhombohedral secondary phases, respectively, in addition to the principle monoclinic phase, which may thus explain the absence of a secondary phase in the present study. It can be noted that the spatial homogeneity of the samples investigated in the present work can be expected to be very similar to those described in previous work[4,13] as the linewidths of the principal reflections (~0.015 Å) are essentially identical.

TABLE III. Microstrain S_{HKL} and Gaussian-Lorentzian mixing coefficient η from the Rietveld refinement of monoclinic *Cm* $PbZr_{0.52}Ti_{0.48}O_3$. The *d*-dependent Gaussian contribution to the linewidth, $\sigma_1=32$ at 280 K.

	$PbZr_{0.52}Ti_{0.48}O_3$
T(K)	280
η	0.516(5)
S_{400}	0.700(11)
S_{040}	0.285(7)
S_{004}	5.36(5)
S_{220}	0.467(8)
S_{202}	−0.513(18)
S_{022}	−0.236(14)
S_{301}	−0.587(13)
S_{103}	1.99(3)
S_{121}	−0.580(17)

Superlattice reflections are present in the diffraction data obtained at 47 and 150 K, indicating a doubling of the monoclinic unit cell as found previously at 10 K.[8,9] These all-odd *hkl* reflections with respect to a doubled elementary perovskite unit cell indicate the presence of an antiphase tilt system.[32] This phase transition from monoclinic *Cm* to monoclinic *Cc* involves antiferrodistortive tilting of the $(Zr,Ti)O_6$ octahedra, leading to cell doubling. The superlattice reflections are essentially due to these oxygen displacements and can be expected to be of extremely low intensity in x-ray diffraction. In the *Cc* phase, which corresponds to a $a^-a^-c^-$ tilt sytem,[33] the rotation angles about axes parallel to the pseudocubic **a** (or **b**) and **c** directions can be calculated, Table IV. It is found that the former ω_a is much smaller that the latter ω_c, which reaches a value of 2.3° at 47 K.

If electronic polarization and domain contributions are neglected, the structural data can be used to calculate the spontaneous polarization along with the polarization rotation angle (θ) with respect to the pseudotetragonal *z* axis in the

TABLE IV. Octahedral tilt angles ($\omega_a, \omega_b, \omega_c$) as a function of P and T for $PbZr_{0.52}Ti_{0.48}O_3$.

P (GPa)	T (K)	ω_a (deg)	ω_b (deg)	ω_c (deg)
0.0001	47	0.15	0.15	2.3
0.0001	150	0.2	0.2	1.7
0.0001	230	0	0	0
0.0001	280	0	0	0
0.7	150	0.5	0.5	2.3
1.1	280	0	0	0
2.4	281	1.1	1.1	2.9
3.8	288	1.6	0.5	3.4
4.9	295	1.5	1.8	2.7
7.2	128	2.5	2.2	5.7
7.1	306	2.5	2	6
7.6	310	2.5	2	6

TABLE V. Spontaneous polarization P_s and rotation angles θ and φ as a function of P and T for $PbZr_{0.52}Ti_{0.48}O_3$.

P (GPa)	T (K)	P_s ($\mu C/cm^2$)	θ (deg)	φ (deg)
0.0001	47	40.3	23.4	0
0.0001	150	39	22.3	0
0.0001	230	38.2	19.3	0
0.0001	280	37.6	19.5	0
0.7	150	38.6	39	0
1.1	280	32.4	18.3	0
2.4	281	27.4	23.5	0
3.8	288	17	30	4
4.9	295	21	71	12
7.2	128	19	67	28
7.1	306	0	-	-
7.6	310	0	-	-

monoclinic phase using the following relationship:[16]

$$\mathbf{P}_s = (1/V)\Sigma_i q_i \mathbf{r}_i, \quad (1)$$

where q_i and $\mathbf{r}_i$ are, respectively, the point charges and their positions in the unit cell of volume V. It can be seen from Table V that the effect of temperature (at $P_{atm}=0.0001$ GPa) from 47 to 280 K is to decrease both the rotation angle θ and P_s. Over this temperature range, only minor variations are observed. At higher temperatures both θ and P_s tend to zero ($\theta \rightarrow 0$ at the monoclinic-tetragonal phase transition[3] near 300 K and $P_s \rightarrow 0$ at the transition[34–36] to the paraelectric cubic phase at 667 K).

B. Variable-pressure, variable-temperature study of $PbZr_{0.52}Ti_{0.48}O_3$

The structure of $PbZr_{0.52}Ti_{0.48}O_3$ could be successfully refined using a monoclinic *Cm* structural model, Tables I and VI, using the neutron diffraction data obtained at 1.1 GPa and 280 K (Fig. 1), as was the case at ambient pressure. The results indicate a slight reduction in the spontaneous polarization, Table V.

The data obtained both at $P=0.7$ GPa, $T=150$ K (Fig. 2) and $P=2.4$ GPa, $T=281$ K indicate a transition to a high-pressure form and confirm that the structure is monoclinic, space group *Cc*, as found at low temperature and ambient pressure. The same all-odd *hkl* superlattice reflections are present, indicating a doubling of the monoclinic unit cell. The superlattice reflections increase in intensity as a function of pressure due to the increased tilting of the $(Zr,Ti)O_6$ octahedra, Table IV. In fact, at 2.4 GPa and higher pressures, *all* the possible all-odd *hkl* superlattice reflections in the *d*-spacing range between 1.3 and 3 Å (311, 331, 333, 511, 533 and their permutations) are clearly visible in the diffraction patterns. The observation of these superlattice reflections confirms the presence of the monoclinic *Cc* form and indicate that cell doubling occurs at a much lower pressure that the 6–7 GPa proposed based on x-ray diffraction and Raman spectroscopy.[24] Recent dielectric measurements[23] indicate a broad hysteresis loop in the pressure range up to 1.8 GPa, which may be linked to the *Cm*-*Cc* phase transition. This is consistent with the first-order nature of the equivalent transition in $PbZr_{0.40}Ti_{0.60}O_3$ occurring at close to 3 GPa with a 0.7% volume change.[23,25] It can also be noted that, based on a close inspection of published Raman spectra,[18,24] the strongest peak related to octahedral tilting in the doubled unit cell[18] actually begins to appear as a weak shoulder in the 360-cm^{-1} region at close to 2 GPa.

A transition from monoclinic *Cm* to rhombohedral *R*3*m* symmetry was proposed to occur in the 2–3 GPa pressure range based on x-ray diffraction data.[24] The present evidence for unit-cell doubling due to octahedral tilting in this pressure range eliminates these two space groups, which are not compatible with such tilting. If there is a tendency towards rhombohedral symmetry above 3 GPa, the space group *R*3*c* (tilt system $a^-a^-a^-$), which is a supergroup of *Cc*, should be considered instead. Various structural models were used for the refinement of the structure using the data obtained at 3.8 GPa and 288 K, including monoclinic *Cc*, rhombohedral *R*3*c*, and triclinic *F*1. The latter group is a direct subgroup of *Cc* and corresponds to the $a^-b^-c^-$ tilt system.[32,33] This structure was found in a recent neutron diffraction study[37] of 7% lanthanum-doped $PbZr_{0.65}Ti_{0.35}O_3$ (PLZT) and it was proposed that this structure may exist in certain regions of the phase diagrams of both the PLZT and PZT systems instead of the *R*3*c* structure. Triclinic forms have also been identified in theoretical calculations.[10,38,39] Of the three candidate structures, the poorest fit was obtained with the *R*3*c* model ($Rwp=3.0\%, Rp=3.1\%$). This was particularly noticeable for the strong pseudocubic 111 and 200 reflections. In *R*3*c* symmetry only the former is split. In the calculated profiles using this model the width of the 111 reflection is systematically overestimated, whereas that of the 200 reflection is underestimated even when a line shape function with microstrain contributions is used. The *R*3*c* model thus does not accurately reproduce the experimental data. The present result is in agreement with previous x-ray diffraction studies,[17,24] which indicate that the cell parameters have not yet merged to a single pseudocubic *a* parameter at 3.8 GPa.

TABLE VI. Fractional atomic coordinates, isotropic (iso), or equivalent (eq) atomic displacement parameters ($Å^2$) and agreement factors (%) for monoclinic and triclinic $PbZr_{0.52}Ti_{0.48}O_3$ as a function of P. Data for WC, Ni, and Pb included in the multiphase refinements are also given. *Cm*: site occupancies Pb, Zr/Ti, O(1) $2a$ $(x,0,z)$, O(2) $4b(x,y,z)$. Origin at Pb position. *Cc*: site occupancies $4a(x,y,z)$. Origin based on Pb x and z coordinates $(0,y,0)$. $F1$: site occupancies $4a(x,y,z)$. Origin at $(0,y\text{Pb-}0.25,0)$ to permit comparison with the coordinates in the $F\bar{1}$structure. $F\bar{1}$: Site occupancies Zr(1)/Ti(1) $4f$ $(0.75,0,0.25)$, Zr(2)/Ti(2) $4c(0.25,0,0.25)$, Pb, O(1), O(2) O(3) $8i(x,y,z)$. Origin at inversion center. Additional phases: WC-$6m2$ W$(0,0,0)$ C $(2/3,1/3,1/2)$, Ni-$Fm\bar{3}m$ Ni $(0,0,0)$, Pb-$Fm\bar{3}m$ Pb$(0,0,0)$. The values obtained for the pressure cell components WC and Ni are not representative of these materials as they are in a highly strained state and in addition are not centered on the diffractometer.

	Cm	*Cc*	*F*1	$F\bar{1}$
T (K)	280	150	288	310
P (GPa)	1.1	0.7	3.8	7.6
y-Pb(1)	0	0.7417(11)	0.25	0.2501(27)
U_{eq}-Pb(1),Pb(2)	0.021(1)	0.020(1)	0.020(3)	0.019(3)
x-Pb(2)			0.01933(9)	
y-Pb(2)			0.7483(20)	
z-Pb(2)			−0.0139(10)	
x-Zr(1),Ti(1)	0.4694(22)	0.2197(8)	0.2425(36)	0.25
y-Zr(1),Ti(1)	0	0.2656(21)	0.0146(29)	0
z-Zr(1),Ti(1)	0.5477(17)	0.2065(12)	0.2722(21)	0.25
U_{iso}-Zr(1),Zr(2)	0.011(1)	0.0058(7)	0.0040(7)	0.0024(5)
U_{iso}-Ti(1),Ti(2)	0.034(3)	0.035(3)	0.041(3)	0.0094(15)
x-Zr(2),Ti(2)			0.7465(35)	0.75
y-Zr(2),Ti(2)			0.0076(40)	0
z-Zr(2),Ti(2)			0.2646(23)	0.25
x-O(1)	0.4657(14)	−0.0377(4)	0.7329(13)	0.7191(5)
y-O(1)	0	0.2474(35)	0.7591(20)	0.7518(28)
z-O(1)	0.0707 (13)	−0.0842(7)	0.2257(13)	0.2592(14)
U_{eq}-O(1)	0.015(2)	0.008(2)	0.017(3)	0.013(2)
x-O(2)	0.2176(12)	0.1969(5)	0.7316(13)	0.7579(22)
y-O(2)	0.2448(11)	0.4841(7)	−0.0033(32)	−0.0121(22)
z-O(2)	0.5905(7)	−0.0977(10)	0.0236(9)	−0.0027(36)
U_{eq}-O(2)	0.014(2)	0.004(1)	0.0065(2)	0.053(4)
x-O(3)		0.2029(5)	0.0077(26)	0.0026(25)
y-O(3)		0.0051(10)	−0.0177(11)	−0.0207(4)
z-O(3)		0.4276(15)	0.2342(18)	0.2590(13)
U_{eq}-O(3)		0.014(1)	0.017(3)	0.011(2)
x-O(4)			0.2272(12)	
y-O(4)			−0.0033(32)	
z-O(4)			0.0163(9)	
U_{eq}-O(4)			0.0065(2)	
x-O(5)			0.7570(18)	
y-O(5)			0.2644(14)	
z-O(5)			0.2547(19)	
U_{eq}-O(5)			0.016(4)	
x-O(6)			0.5099(24)	
y-O(6)			0.0166(12)	
z-O(6)			0.2312(16)	
U_{eq}-O(6)			0.016(4)	
a_{WC} (Å)	2.8997(5)	2.9012(4)	2.8931(5)	2.8900(5)

TABLE VI. (*Continued.*)

	Cm	*Cc*	*F*1	$F\bar{1}$
c_{WC} (Å)	2.8344(8)	2.8294(6)	2.8346(8)	2.8233(8)
U_{iso}-W	−0.0075(9)	−0.0069(7)	−0.0060(9)	−0.008(1)
U_{iso}-C	−0.0016(8)	−0.0022(6)	−0.0052(6)	−0.0039(8)
a_{Ni} (Å)	3.5250(8)	3.5320(6)	3.5289(8)	3.5169(8)
U_{iso}-Ni	0.001(1)	−0.0027(6)	0.0006(9)	0.002(1)
a_{Pb} (Å)	4.908(2)	4.908(1)	4.830(1)	4.745(2)
U_{iso}-Pb	0.011(3)	0.014(3)	0.006(2)	0.006(2)
R_{wp}	3.0	2.6	2.5	2.4
R_p	3.0	2.6	2.4	2.2

In contrast to the above, the best fit was obtained with the triclinic *F*1 model ($Rwp=2.5\%, Rp=2.4\%$), Fig. 3. In this structure, the tilt angles ω_a and ω_b are no longer required to be equal as in the monoclinic *Cc* phase and the spontaneous polarization can now adopt any given orientation. This orientation can be described using a second rotation angle φ (calculated from the spontaneous polarization components $P_{s(x)}$ and $P_{s(y)}$) in addition to θ. The angle φ is defined as the rotation angle in the *xy* plane with respect to the *x* axis in the monoclinic *Cm* phase (i.e., $\varphi=0°$), which is equivalent to the [110] direction in both the primitive cubic perovskite structure and in the triclinic *F*1 structure. Such a triclinic structure is particularly interesting with respect to its piezoelectric response as the polarization vector can adopt any orientation in space. It can therefore align itself with an electric field via a polarization rotation mechanism without the requirement for electric-field-induced phase transitions with their corresponding energy barriers. It may also be noted that the *F*1 (or *P*1) space group is the only group in which there are no nonpolar directions.

A significant reduction in line broadening was observed with increasing pressure. The data obtained at 3.8 GPa were essentially limited by the instrumental resolution. This reduction in linewidth can be linked to decreased microstrain broadening due to a lower susceptibility to spatial inhomogeneity of Zr/Ti (Refs. 13 and 14) for the crystal structures present at high pressure and to less diffuse scattering linked to disorder (primarily due to off-center lead displacements) with respect to that existing in the monoclinic *Cm* phase in the present sample at lower pressures. The recent results on the tetragonal composition $PbZr_{0.40}Ti_{0.60}O_3$ at high pressure support the presence of these two phenomena in the *Cm* form as, in contrast to the present work on $PbZr_{0.52}Ti_{0.48}O_3$, the neutron diffraction linewidths were found to *increase* with pressure[25] as a consequence of the *P*4*mm*-*Cm* phase transition. The presence of significant disorder in the *Cm* phase of $PbZr_{0.52}Ti_{0.48}O_3$ is also supported by theoretical calculations,[40] which indicate the presence of contributions from phonons at points lying outside the center of the Brillouin zone. The data obtained at 4.9 GPa and 295 K and at low temperature (7.2 GPa, 128 K) were also fitted with the best agreement factors using an *F*1 structural model.

Previous x-ray diffraction studies[17,24] indicated that at close to 5 GPa at room temperature, the unit cell of $PbZr_{0.52}Ti_{0.48}O_3$ is strongly pseudocubic. At this pressure, several Raman modes in 125–145 cm^{-1} region were found to disappear[17,18] as was the case for the transition to the cubic paraelectric phase at ambient pressure and high temperature.[41] It can be noted that for the ferroelectric phases, the Raman spectra are similar, and in contrast to what occurs at the transition at 5 GPa, new modes appear at the various transitions.[18,25] The disappearance of modes at

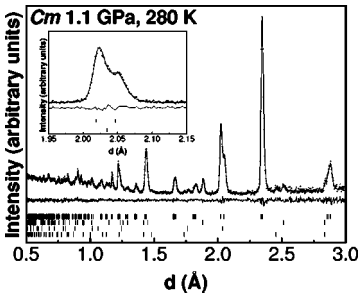

FIG. 1. Experimental and calculated profiles from the Rietveld refinement of the monoclinic *Cm* phase of $PbZr_{0.52}Ti_{0.48}O_3$ at 1.1 GPa and 280 K. The difference profile is on the same scale. Vertical ticks indicate, from the top down, the calculated positions of the *Cm* phase, tungsten carbide and nickel from the anvils of the pressure cell and lead.

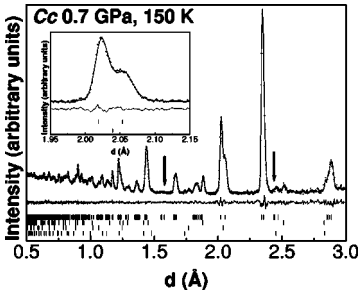

FIG. 2. Experimental and calculated profiles from the Rietveld refinement of the monoclinic *Cc* phase of $PbZr_{0.52}Ti_{0.48}O_3$ at 0.7 GPa and 150 K. The difference profile is on the same scale. Vertical ticks indicate, from the top down, the calculated positions of the *Cc* phase, tungsten carbide and nickel from the anvils of the pressure cell and lead. Arrows indicate the most prominent superlattice reflections.

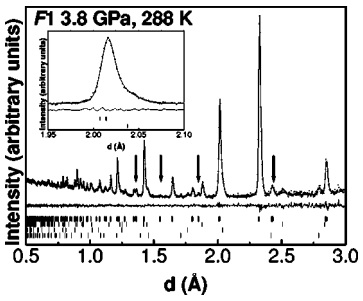

FIG. 3. Experimental and calculated profiles from the Rietveld refinement of the triclinic $F1$ phase of $PbZr_{0.52}Ti_{0.48}O_3$ at 3.8 GPa and 288 K. The difference profile is on the same scale. Vertical ticks indicate, from the top down, the calculated positions of the $F1$ phase, tungsten carbide and nickel from the anvils of the pressure cell and lead. Arrows indicate the most prominent superlattice reflections.

5 GPa and the similarity with respect to the high-temperature behavior[41] give supporting evidence for a transition from a polar, noncentrosymmetric group to a nonpolar, centrosymmetric group. Cubic symmetry is, however, incompatible with the antiphase tilting, which gives rise to the superlattice reflections found in the present study. A centrosymmetric $F\bar{1}$ model structure was thus also tested for the points obtained above this pressure in the 306–310 K temperature range. The agreement factors obtained with this structural model ($Rwp=2.4\%, Rp=2.2\%$), Fig. 4, at the highest pressure (7.6 GPa, 310 K) are equivalent to those obtained using the polar $F1$ space group. In this structure, Fig. 5, the Zr, Ti cations are located on inversion centers and the constituent octahedra are tilted about directions parallel to **a**, **b**, and **c**.

C. Polarization rotation and octahedral tilting at high pressure

The phase transition behavior of $PbZr_{0.52}Ti_{0.48}O_3$ as a function of pressure and temperature is dominated by the rotation and reduction of the spontaneous polarization and by octahedral tilting, Tables IV and V. Polarization rotation is

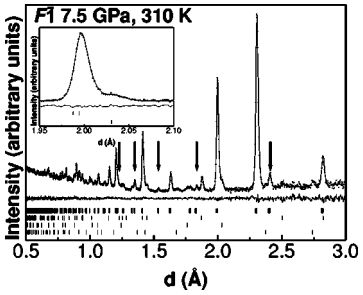

FIG. 4. Experimental and calculated profiles from the Rietveld refinement of the triclinic $F\bar{1}$ phase of $PbZr_{0.52}Ti_{0.48}O_3$ at 7.6 GPa and 310 K. The difference profile is on the same scale. Vertical ticks indicate, from the top down, the calculated positions of the $F\bar{1}$ phase, tungsten carbide and nickel from the anvils of the pressure cell and lead. Arrows indicate the most prominent superlattice reflections.

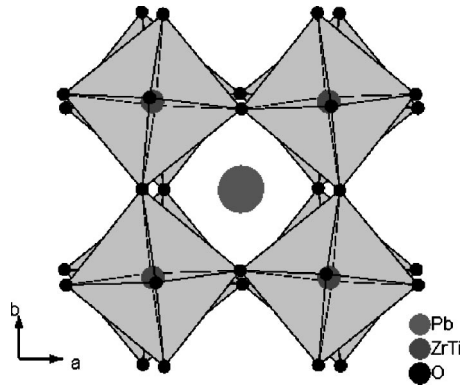

FIG. 5. Crystal structure of the triclinic $F\bar{1}$ phase of $PbZr_{0.52}Ti_{0.48}O_3$.

active at low temperature and ambient pressure. High pressure is also shown to drive this process. It should be noted that, whereas polarization rotation decreases as a function of temperature and increases as a function of pressure, the magnitude of P_s decreases as a function of P and T. Particularly high values of θ are obtained at high pressure in the $F1$ phase. Furthermore, an additional degree of freedom is allowed: rotation in the xy plane described by the angle φ. The θ values obtained at the two highest pressures for the $F1$ phase, Table V, are very close to that corresponding to the pseudocubic [112] direction ($\theta=70.5°$). This indicates that the rotation of the in-plane component (i.e., θ angle) of the spontaneous polarization occurs principally between the [001] and [112] directions and is not limited to the pathway between the [001] and the [111] direction ($\theta=54.7°$), corresponding to rhombohedral symmetry, as proposed previously.[5] In the recent study[37] of the $F1$ structure in PLZT, the polarization direction was also found to lie close to [112], and it was proposed that the observed domain morphology[42,43] may be explained by the complex domain structure due to the change in polarization direction between equivalent ⟨112⟩ directions. In addition, such a domain structure indicates that the triclinic phase may extend to compositions with lower La content. This prediction is verified by the present study as this phase is shown to occur for pure, undoped PZT at high pressure.

The spontaneous polarization decreases as a function of increasing temperature and/or pressure indicating a tendency towards a paraelectric state. A centrosymmetric structure is obtained at the highest pressures at room temperature corresponding to the $F\bar{1}$ phase. It can be noted, however, that broad features are still present in the Raman spectrum of this phase[17,18,24] in addition to the sharp bands characteristic of an ordered form. This may be evidence for the persistence of $F1$-like "polar nanoregions" (PNR) (Refs. 44–46) in the "paraelectric" phase. Whereas the sharp bands persist, these broad features slowly decrease in intensity with further increases in pressure corresponding to the reduction in size and gradual disappearance of these PNR's.

Octahedral tilting is already present at ambient pressure at temperatures below 210 K in the monoclinic Cc phase[7–9] ($a^-a^-c^-$ tilt sytem) in $PbZr_{0.52}Ti_{0.48}O_3$. Polyhedral tilting in general can be an efficient compression mechanism in the

TABLE VII. Polyhedral interatomic distances (Å) for monoclinic and triclinic $PbZr_{0.52}Ti_{0.48}O_3$ as a function of *P*.

	Cm	*Cm*	*Cc*	*F*1	$F\bar{1}$
T (K)	280	280	150	288	310
P (GPa)	0.0001	1.1	0.7	3.8	7.6
Pb-O_1	2.495(1)	2.517(5)	2.383(5)	2.610(10); 2.614(24)	2.599(8)
Pb-O_2	2.495(1)	2.517(5)	2.591(7)	2.726(20); 2.665(25)	2.655(17)
Pb-O_3	2.707(2)	2.674(8)	2.611(5)	2.741(20); 2.717(17)	2.706(9)
Pb-O_4	2.685(1)	2.739(6)	2.703(8)	2.835(11); 2.719(13)	2.709(23)
Pb-O_5	2.685(1)	2.739(6)	2.753(7)	2.843(15); 2.741(17)	2.750(16)
Pb-O_6	2.883(2)	2.876(8)	2.848(21)	2.844(13); 2.817(17)	2.790(23)
Pb-O_7	2.883(2)	2.876(8)	2.912(21)	2.861(12); 2.888(17)	2.837(24)
Pb-O_8	3.144(1)	3.051(5)	3.074(6)	2.864(12); 2.943(18)	2.879(18)
Pb-O_9	3.144(1)	3.051(5)	3.089(7)	2.870(15); 2.981(17)	2.933(23)
Pb-O_{10}	3.054(2)	3.067(8)	3.144(5)	2.964(19); 3.015(13)	2.950(8)
Pb-O_{11}	3.318(1)	3.258(5)	3.210(6)	2.975(19); 3.076(22)	2.992(17)
Pb-O_{12}	3.318(1)	3.258(5)	3.397(5)	3.081(10); 3.112(22)	3.052(8)
Pb-O_m	2.901(1)	2.885(6)	2.893(9)	2.854(17)	2.814(16)
Ti,Zr-O_1	1.968(2)	1.953(9)	1.906(12)	1.933(28); 1.927(34)	1.990(22); 1.977(29)
Ti,Zr-O_2	2.016(3)	2.014(11)	2.002(8)	2.001(28); 1.946(20)	1.990(22); 1.977(29)
Ti,Zr-O_3	2.016(3)	2.014(11)	2.018(13)	2.017(26); 2.020(40)	2.019(29); 1.981(20)
Ti,Zr-O_4	2.045(3)	2.040(11)	2.045(11)	2.033(18); 2.036(20)	2.019(29); 1.981(20)
Ti,Zr-O_5	2.045(3)	2.040(11)	2.127(7)	2.069(18); 2.065(34)	2.024(20); 2.019(22)
Ti,Zr-O_6	2.169(2)	2.142(9)	2.157(13)	2.181(34); 2.130(35)	2.024(20); 2.019(22)
Ti,Zr-O_m	2.043(3)	2.034(10)	2.043(11)	2.030(29)	2.002(24)

Two distance values are given in triclinic symmetry, in which there are two inequivalent AO_{12} [Pb(1),Pb(2)] and/or BO_6 [Zr(1),Ti(1);Zr(2),Ti(2)] polyhedra.

ABO_3 perovskite structures provided that there is a difference in compressibility between the AO_{12} and BO_6 polyhedra.[47] If the AO_{12} polyhedra are more compressible, octahedral tilting is predicted to increase, whereas in the case of less compressible AO_{12} polyhedra, octahedral tilting decreases with pressure. This will also depend on the value of the tolerance factor[48] $t=d_{A\text{-}O}/(2^{1/2})d_{B\text{-}O}$. In the case of an undistorted perovskite $t=1$, whereas octahedral tilting is expected to be present for $t<1$ as the *A* cation is too small for *A*-cation site in the perovskite structure. The compressibility of the average Pb-O distance in the PbO_{12} polyhedron is 50% greater than that of the average (Zr,Ti)-O distance in the $(Zr,Ti)O_6$ octahedron for $PbZr_{0.52}Ti_{0.48}O_3$, Table VII. It can be noted that for $PbZr_{0.52}Ti_{0.48}O_3$ at ambient temperature and pressure, *t* is very close to the limiting value of 1 (observed value $t=1.004$). At the highest pressure reached, this value decreased to 0.994. It can thus be expected that octahedral tilting will act as an important compression mechanism. This is true at low temperatures ($T<210$ K) over the entire pressure range investigated and at higher temperatures beginning at the *Cm*-*Cc* transition pressure above 1.1 GPa. In the triclinic *F*1 and $F\bar{1}$ phases, although the tilt system is $a^-b^-c^-$, the actual tilt configuration with $\omega_c \gg \omega_a, \omega_b$ is very similar to that present in the *Cc* phase. Thus, even at the highest pressure the structure does not approach rhombohedral *R*3*c* symmetry, in which all three tilt angles are required to be identical.

The present results permit an updated *P*-*T* phase diagram of $PbZr_{0.52}Ti_{0.48}O_3$ to be proposed, Fig. 6. Two phase boundaries have been measured experimentally. The *P*4*mm*-$Pm\bar{3}m$ phase boundary was shown to be negative by dielectric measurements[49,50] up to 0.8 GPa. The boundary separating the paraelectric high-pressure $F\bar{1}$ phase from the lower-pressure ferroelectric phases was obtained from x-ray diffraction[17] and Raman scattering results.[17,18] The present

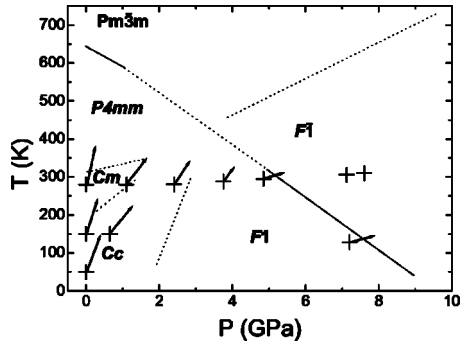

FIG. 6. Pressure-temperature phase diagram of $PbZr_{0.52}Ti_{0.48}O_3$. The solid lines represent phase boundaries obtained from x-ray diffraction, Raman spectroscopy, and dielectric measurements. Dashed lines correspond to proposed *P*-*T* boundaries. Neutron diffraction data are represented by (+) along with the in-plane contribution (φ not shown) to the calculated spontaneous polarization vector.

neutron diffraction results establish certain points in *P-T* space, where these ferroelectric phases were found to be present. Possible phase boundaries are thus proposed based on these data. The low-temperature section of the boundary between the *Cc* and *F*1 phases is supported by changes, which are found at low pressure in the published Raman spectra obtained at 44 and 154 K.[18] A hypothetical F_1 -$Pm\bar{3}m$ phase boundary is proposed with a positive slope as, due to the increase in tilt angle in the $F\bar{1}$ phase as a function of pressure, more thermal energy will be required to return to an undistorted cubic perovskite structure. The polarization rotation mechanism and the associated reduction in polarization as a function of *T* and *P* are also clearly evident from the polarization vectors given for each point corresponding to a structure refined by neutron diffraction.

IV. CONCLUSIONS

The crystal structure of $PbZr_{0.52}Ti_{0.48}O_3$ was refined at 12 points in the *P-T* phase diagram of this material. A series of low-symmetry monoclinic (Cm, Cc) and triclinic $(F1, F\bar{1})$ structures are identified for $PbZr_{0.52}Ti_{0.48}O_3$ as a function of pressure. However, no transitions to rhombohedral or cubic forms were observed. The high-pressure structure present above 6 GPa is centrosymmetric and triclinic. The principle compression mechanisms active at high pressure are the rotation and reduction of the spontaneous polarization and tilting of the $(Zr, Ti)O_6$ octahedra. Low temperature and high pressure have similar but contrasting effects on $PbZr_{0.52}Ti_{0.48}O_3$. In both cases, polarization rotation and octahedral tilting increase; however, the magnitude of the spontaneous polarization increases with decreasing temperature, but decreases at high pressure. The combined effect of these mechanisms leads to the observed complex phase diagram of this material involving a number of low-symmetry structures.

ACKNOWLEDGMENT

We would like to thank D.J. Francis (ISIS) for technical assistance with the Paris-Edinburgh pressure cell.

*Author to whom correspondence should be addressed. Electronic address: jhaines@lpmc.univ-montp2.fr

[1] B. Jaffe, W. R. Cook, and H. Jaffe, *Piezoelectric Ceramics* (Academic, London, 1971).
[2] B. Noheda, D. E. Cox, G. Shirane, J. A. Gonzalo, L. E. Cross, and S.-E. Park, Appl. Phys. Lett. **74**, 2059 (1999).
[3] B. Noheda, J. A. Gonzalo, L. E. Cross, R. Guo, S.-E. Park, D. E. Cox, and G. Shirane, Phys. Rev. B **61**, 8687 (2000).
[4] B. Noheda, D. E. Cox, G. Shirane, R. Guo, B. Jones, and L. E. Cross, Phys. Rev. B **63**, 014103 (2000).
[5] R. Guo, L. E. Cross, S.-E. Park, B. Noheda, D. E. Cox, and G. Shirane, Phys. Rev. Lett. **84**, 5423 (2000).
[6] H. Fu and R. E. Cohen, Nature (London) **403**, 281 (2000).
[7] Ragini, S. K. Mishra, D. Pandey, H. Lemmens, and G. Van Tendeloo, Phys. Rev. B **64**, 054101 (2001).
[8] R. Ranjan, Ragini, S. K. Mishra, D. Pandey, and B. J. Kennedy, Phys. Rev. B **65**, 060102 (2002).
[9] D. M. Hatch, H . T. Stokes, R. Ranjan, Ragini, S. K. Mishra, D. Pandey, and B. J. Kennedy, Phys. Rev. B **65**, 212101 (2002).
[10] D. Vanderbilt and M. H. Cohen, Phys. Rev. B **63**, 094108 (2001).
[11] J. Frantti, S. Ivanov, J. Lappalainen, S. Eriksson, V. Lantto, S. Nishio, K. Kakihana, and H. Rudlöf, Ferroelectrics **266**, 73 (2002).
[12] A. M. Glazer, P. A. Thomas, K. Z. Baba-Kishi, G. K. H. Pang, and C. W. Tai, Phys. Rev. B **70**, 184123 (2004).
[13] J. Frantti, S. Eriksson, S. Hull, V. Lantto, H. Rudlöf, and K. Kakihana, J. Phys.: Condens. Matter **15**, 6031 (2003).
[14] J. Frantti, S. Eriksson, S. Hull, S. Ivanov, V. Lantto, J. Lappalainen, and K. Kakihana, J. Eur. Ceram. Soc. **24**, 1141 (2004).
[15] J. Frantti, J. Lappalainen, S. Eriksson, V. Lantto, S. Nishio, K. Kakihana, S. Ivanov, and H. Rudlöf, Jpn. J. Appl. Phys., Part 1 **39**, 5697 (2000).
[16] J. Frantti, S. Ivanov, S. Eriksson, H. Rudlöf, V. Lantto, J. Lappalainen, and K. Kakihana, Phys. Rev. B **66**, 064108 (2002).
[17] J. Rouquette, J. Haines, V. Bornand, M. Pintard, Ph. Papet, R. Astier, J. M. Léger, and F. Gorelli, Phys. Rev. B **65**, 214102 (2002).
[18] J. Rouquette, J. Haines, V. Bornand, M. Pintard, Ph. Papet, B. Bonnet, and F. A. Gorelli, Solid State Sci. **5**, 451 (2003).
[19] J. Rouquette, V. Bornand, J. Haines, Ph. Papet, and F. Gorelli, Integr. Ferroelectr. **48**, 53 (2002).
[20] J. Haines, J. Rouquette, V. Bornand, M. Pintard, Ph. Papet, and F. A. Gorelli, J. Raman Spectrosc. **34**, 519 (2003).
[21] J. Rouquette, V. Bornand, J. Haines, M. Pintard, and Ph. Papet, Ferroelectrics **288**, 147 (2003).
[22] J. Rouquette, J. Haines, V. Bornand, M. Pintard, and Ph. Papet, J. Phys. IV **113**, 143 (2004).
[23] Ph. Papet, J. Rouquette, V. Bornand, J. Haines, M. Pintard, and P. Armand, J. Electroceram. (to be published).
[24] A. Sani, B. Noheda, I. A. Kornev, L. Bellaiche, P. Bouvier, and J. Kreisel, Phys. Rev. B **69**, 020105(R) (2004).
[25] J. Rouquette, J. Haines, V. Bornand, M. Pintard, Ph. Papet, C. Bousquet, L. Konczewicz, F. A. Gorelli, and S. Hull, Phys. Rev. B **70**, 014108 (2004).
[26] M. Fornari and D. J. Singh, Phys. Rev. B **63**, 092101 (2001).
[27] H. T. Stokes, E. H. Kisi, D. M. Hatch, and C. J. Howard, Acta Crystallogr., Sect. B: Struct. Sci. **58**, 934 (2002).
[28] A. D. Fortes, Ph.D. thesis, University College London, 2004, pp. 170–171, and references therein.
[29] F. Birch, Phys. Rev. **71**, 809 (1947).
[30] A. C. Larson and R. B. Von Dreele, *GSAS: General Structure Analysis System* (Los Alamos National Laboratory, Los Alamos NM, 1994).
[31] P. W. Stephens, J. Appl. Crystallogr. **32**, 281 (1999).
[32] A. M. Glazer, Acta Crystallogr., Sect. A: Cryst. Phys., Diffr., Theor. Gen. Crystallogr. **31**, 756 (1975).
[33] A. M. Glazer, Acta Crystallogr., Sect. B: Struct. Crystallogr. Cryst. Chem. **28**, 3384 (1972).

[34] S. K. Mishra, A. P. Singh, and D. Pandey, Appl. Phys. Lett. **69**, 1707 (1996).
[35] S. K. Mishra, A. P. Singh, and D. Pandey, Philos. Mag. B **76**, 213 (1997).
[36] S . K. Mishra, A. P. Singh, and D. Pandey, Philos. Mag. B **76**, 227 (1997).
[37] H. Liu, R. Harrison, and A. Putnis, J. Appl. Phys. **90**, 6321 (2001).
[38] I. A. Sergienko, Yu. M. Gufan, and S. Urazhdin, Phys. Rev. B **65**, 144104 (2002).
[39] N. Huang, Z. Liu, Z. Wu, W. Duan, B.-L. Gu, and X.-W. Zhang, Phys. Rev. Lett. **91**, 067602 (2003).
[40] A . M. George, J. Iniguez, and L. Bellaiche, Phys. Rev. B **65**, 180301 (2002).
[41] J. Frantti and V. Lantto, Phys. Rev. B **56**, 221 (1997).
[42] M. A. Akbas, I. M. Reaney, and W. E. Lee, J. Mater. Res. **11**, 2293 (1996).
[43] D. Viehland, X. Dai, and Z. Xu, J. Appl. Phys. **84**, 458 (1998).
[44] H. Uwe, K. B. Lyons, H. L. Carter, and P. A. Fleury, Phys. Rev. B **33**, 6436 (1986).
[45] P. DiAntonio, B. E. Vugmeister, J. Toulouse, and L. A. Boatner, Phys. Rev. B **47**, 5629 (1993).
[46] J. Toulouse, P. DiAntonio, B. E. Vugmeister, X. M. Wang, and L. A. Knauss, Phys. Rev. Lett. **68**, 232 (1992).
[47] J. Zhou, N. L. Ross, and R. J. Angel, Acta Crystallogr., Sect. B: Struct. Sci. **60**, 263 (2004).
[48] V. M. Goldschmidt, Naturwissenschaften **14**, 477 (1926).
[49] M. Pisarski, Ferroelectrics **81**, 297 (1988).
[50] M. Pisarski, Ferroelectrics **94**, 215 (1989).